Energy & Environmental Science

Cite this: *Energy Environ. Sci.*, 2011, **4**, 914

www.rsc.org/ees

PAPER

Titanium-embedded layered double hydroxides as highly efficient water oxidation photocatalysts under visible light†

Yeob Lee, Jung Hoon Choi, Hyung Joon Jeon, Kyung Min Choi, Jung Woo Lee and Jeung Ku Kang*

Received 20th July 2010, Accepted 11th November 2010
DOI: 10.1039/c0ee00285b

Here, we have synthesized the new titanium-embedded layered double hydroxides (LDHs), such as (Ni/Ti)LDH and (Cu/Ti)LDH. First of all, the formation of LDH structures and the bonding nature for a mixed oxide structure of LDHs are explored in this work. Also, it is determined that our LDHs show two absorption bands in the red and blue regions under visible light, thus different from those of a pure titanium oxide with absorption bands in only the UV region. We find that the (Ni/Ti)LDH with the high surface area showed a higher reaction rate, producing 49 μmol O_2 in water oxidation by using 200 mg of the photocatalyst and 1 mmol of $AgNO_3$ as a sacrificial agent. Also, the (Cu/Ti)LDH showed a good reaction rate and produced 31 μmol of O_2 under the same condition. On the other hand, conventional TiO_2 nanoparticles generated a very small amount of oxygen within the error range under this visible light irradiation. Consequently, these results imply that absorption bands in the visible range and the large surface area of an LDH could result in the high water oxidation photocatalytic activity under visible light.

Introduction

Because the current global energy consumption is primarily based on the combustion of fossil fuels that results in pollution and climate change on the earth, the idea of the artificial photosynthesis is considered as an appealing method to produce sustainable fuels from water and carbon dioxide.[1,2] The artificial photosynthesis consists of two critical steps, where the first one is water oxidation and the second one is the conversion of CO_2 into hydrocarbon fuels such as methane and ethanol using protons generated in the water oxidation.[3–5] Among these, visible and ultraviolet light are used for artificial photosynthesis.[6–11] Because the energy of visible light is much higher than the energy of ultraviolet light at the earth's surface, the photocatalytic reaction can be performed under visible light in order to use solar energy with a maximum efficiency.

Although a titanium oxide based photocatalyst[12] has shown a high efficiency for water splitting under UV light, they are inefficient under visible light due to their large bandgap energy. Therefore, atomic substitutional doping methods using anion elements such as N, S, and C have been suggested to narrow the bandgap energy.[13–16] However, these materials show still

KAIST, Graduate School of EEWS, Department of Materials and Science, NanoCentury KAIST Institute, 373-1, Guseong Dong, Yuseong Gu, Daejeon, Republic of Korea. E-mail: jeungku@kaist.ac.kr; Fax: +82-42-350-3310; Tel: +82-42-350-3338

† Electronic supplementary information (ESI) available: Details of pore size distribution of photocatalysts, amounts of evolved oxygen on photocatalysts, oxygen K-edged NEXAFS data for photocatalysts. See DOI: 10.1039/c0ee00285b

Broader context

Because the current global energy consumption is primarily based on the combustion of fossil fuels resulting in pollution and global climate change, artificial photosynthesis consisting of two steps, where the first step is water oxidation and the second one is the conversion of carbon dioxide into hydrocarbon fuels, such as methanol, using protons generated in the water oxidation, is an appealing method to produce sustainable fuels. Here, we report that new titanium embedded layered double hydroxides (LDHs) with large surface areas, such as the (Ni/Ti) LDH and the (Cu/Ti) LDH, are very efficient for water oxidation under visible light. On the other hand, conventional titanium oxide (TiO_2) nanoparticles generated a very small amount of oxygen within the error range under the visible light irradiation. The two kinds of LDHs show two absorption bands in the red and blue regions under visible light, thus different from those of a pure metal oxide with absorption bands in only the UV region. Consequently, these results imply that absorption bands in the visible range and the large surface area of an LDH could result in the high water oxidation photocatalytic activity under visible light.

marginal efficiencies in water oxidation under visible light compared to the performance required for the practical applications.

Meanwhile, Frei *et al.* introduced the metal oxo-bridging structure and their mechanism of photocatalytic effect several years ago.[17–19] Also, they invented metal oxo-bridged photocatalysts, such as Ti–O–Cu, Cr–O–Ir and Zr–O–Cu, using the concept of the metal-to-metal charge transfer (MMCT). This covalent anchoring of metal centers, which introduces new energy levels inside the bandgap, was proven to allow greater extension of the photoactive region in the visible light range. However, the photocatalytic activity under visible light of these materials still show low efficiencies because they only have a small number of metal-oxygen-metal sites that are able to serve as water splitting sites. Furthermore, the formation of attendant providing effective charge-carrier recombination centers has also yet remained unsolved.[20] Moreover, Garcia *et al.* discovered three kinds of Zn(II) based layered double hydroxides (LDHs) for the photocatalysts.[21] However, zinc oxide has a degree of instability due to the photocorrosion under bandgap excitation.[22] The zinc oxide is decomposed into zinc ion and oxygen due to its reaction with holes generated through the photon absorption of

$$ZnO + 2h^+ \rightarrow Zn^{2+} + \tfrac{1}{2}O_2 \quad (1)$$

Herein, we focused on Ti embedded LDHs as candidates for water oxidation catalysts under visible light because titanium oxide is very stable under bandgap excitation and shows good efficiency under UV light.[12,22] The wide band gap which is the biggest problem of titanium oxide is solved by reconstructing bandgap by introducing large amounts of metal-oxygen-metal sites. The scheme of the titanium embedded LDH is illustrated in Fig. 1.

Experimental

Preparation

The LDHs were prepared by the continuous supply of ammonia by decomposition of urea in water at the reflux condition. Also, nickel chloride (98%), copper nitrate (99–104%) and titanium propoxide (98%) were used as metal precursors. Two metal precursors were poured into an aqueous 0.5 M urea (98%) solution for each LDH with a constant ratio of divalent metal ions and tetravalent metal ions ($M^{II+} : M^{IV+} = 6 : 1$). The suspensions were annealed for 2 days at 90 °C and then the green colored powders were obtained through centrifugation at 7000 rpm for 20 min. Then, the powders were washed several times using water and dried at 60 °C overnight.

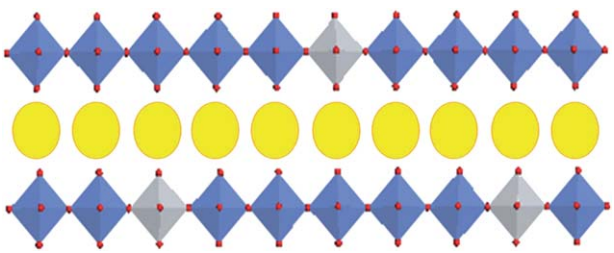

Fig. 1 Scheme of (M^{II}/Ti)LDH structure. Blue octahedron: M^{II}, silver octahedron: Ti^{4+}, red sphere: O, yellow circle: interlayer anion.

Characterization

The powder X-ray diffraction of the samples was obtained with Cu Kα radiation, at a step size of 0.01° and scan speed of 0.8° min^{-1}. The FT-IR spectra were recorded on a Bomem MB154 FT-IR spectrometer with the samples being pressed into KBr pellets. The elemental chemical analysis for the metals was carried out using inductively coupled plasma mass spectroscopy. The XPS data were obtained using an ESCALAB 250 XPS spectrometer in 'flood gun' mode to compensate for the charge-up effect of insulating samples. The low-temperature N_2 adsorption-desorption measurements were carried out using a Quantachrome Autosorb-6 system. The samples were degassed for 1 day at 150 °C before the analysis. The specific surface area was calculated using the Brunauer-Emmett-Teller (BET) method based on the absorption isotherm. The solid state UV-vis diffuse reflectance spectra were recorded at room temperature and in air with a JASCO V-570 spectrometer. The transmission electron microscopy was performed using an FEI Tecnai G2 F30 system coupled with EDAX.

Photocatalytic ability test

The photocatalytic analysis was conducted in a 125 mL Pyrex flask containing 100 mL of an aqueous suspension. The headspace was connected to the inverted burette which was filled with water at atmospheric pressure to make a closed system. The photocatalyst was degassed overnight in a Schlenk line under vacuum and refilled with Ar before being transferred to the reactor. The aqueous suspension was composed of 200 mg of the photocatalyst powder and 1 mmol of $AgNO_3$ (99%) as sacrificial agent. The suspensions were purged with Ar for 1 h to remove the remaining atmospheric air in the reactor. Then, the reactor was irradiated with a 300 W xenon lamp. Two types of filters (UV light filter and IR filter) were used for a visible light irradiation (400 nm < λ < 700 nm). 0.5 mL of the gas was periodically captured from the headspace of the reactor and then directly injected into a gas chromatograph to confirm the production of oxygen evolving from the photocatalytic reaction. The gas chromatograph was operated under isothermal conditions (60 °C) using a packed column (5 Å molecular sieve, 3 mm diameter, 3 m length) equipped with a thermal conductivity detector. Ar gas was used for the carrier gas of the gas chromatograph.

Results and discussion

The layered structure of the materials was proved by the powder X-ray diffraction (PXRD) measurement, as illustrated in Fig. 2. The {003} peaks attributed to the diffraction patterns of the layered structure are observed in both of the two LDHs. In the case of the (Ni/Ti)LDH, the PXRD pattern seen in Fig. 2(a) indicates that (003), (006), (009), (012) and (110) peaks are located at 12°, 24°, 33°, 37° and 60°, respectively, which also exhibit narrow and symmetric peaks at low 2θ in addition to less symmetric peaks at high 2θ.[23] The interlayer spacing is 0.73 nm, which was calculated from (003) reflection for the (Ni/Ti)LDH.

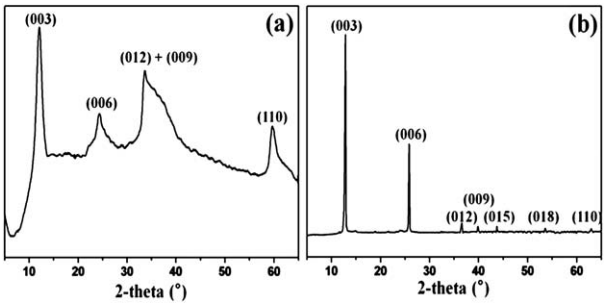

Fig. 2 X-Ray diffraction patterns of (a) (Ni/Ti)LDH and (b) (Cu/Ti)LDH.

Fig. 2(b) shows that the (Cu/Ti)LDH also has a layered structure like that of the (Ni/Ti)LDH. The (003), (006), (012), (009), (015), (018) and (110) peaks were reflected at 13°, 26°, 36°, 40°, 44°, 53° and 63° respectively. The interlayer spacing of 0.69 nm is calculated from the (003) reflection. It is found that the (Ni/Ti)LDH shows broad peaks compared to the (Cu/Ti)LDH. This implies that the (Ni/Ti)LDH is in a partially disordered crystalline structure.

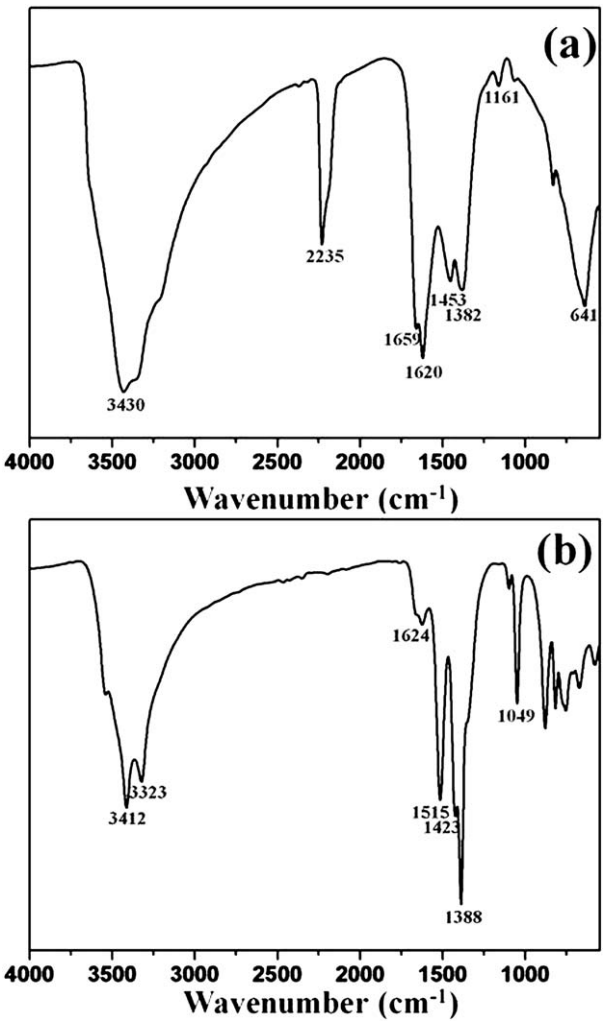

Fig. 3 FT-IR spectra of (a) (Ni/Ti)LDH and (b) (Cu/Ti)LDH.

FT-IR spectroscopy is used to establish the layered double hydroxide structure by identifying the interlayer anions and their influences to materials. The results are illustrated in Fig. 3. In the case of (Ni/Ti)LDH, there is a strong broad band with its center at 3430 cm^{-1}, indicating that there exists a O–H bond. Meanwhile, we find that the peak of the hydroxyl group was shifted to a lower frequency compared to that of the (M^{II}/M^{III})LDH. This is attributed to the change of the electron density on the O–H bond by Ti^{4+}.[24,25] The broadness of the O–H band is also considered to result from the presence of the hydrogen bonding between water molecules and anions in the interlayer gap. The strong band at 2235 cm^{-1} indicates the presence of cyanate (CNO^-) anions. The medium bands, split into two bands at 1659 cm^{-1} and 1620 cm^{-1} and at 1453 cm^{-1} and 1382 cm^{-1}, demonstrate the presence of carbonate (CO_3^{2-}) anion in the interlayer space. The bands at 1659 cm^{-1} and 1620 cm^{-1} indicate the presence of a double bond between C and O while those at 1453 cm^{-1} and 1382 cm^{-1} indicate the presence of a single bond between C and O. The carbonate anion consists of one CO double bond and two CO single bonds. The splitting of two bands occurs from the restricted symmetry in the interlayer space. The tetravalent titanium cation of the layer makes a strong electrostatic attraction between the layer and the interlayer carbonate anion, influencing the symmetries of the interlayer anions. The weak bond at 1161 cm^{-1} is ascribed to the bending mode of the carbonate ions. The band observed at 641 cm^{-1} can be attributed to the overlap of the asymmetric vibration of CO_3^{2-} and to M–O stretching vibration.

The similar phenomena are observed in the (Cu/Ti)LDH. As shown in Fig. 3(b), there are some peaks indicating the presence of carbonate ions, located at 1624 cm^{-1} and 1515 cm^{-1} and at 1423 cm^{-1} and 1388 cm^{-1}. The intensity difference between the two bands shows that the (Cu/Ti)LDH has more CO single bonds than CO double bonds. This is because the charge neutrality between the layers is balanced by only the carbonate anions. The bands found at 500–900 cm^{-1} are attributed to the lattice vibration modes of M–O and M–OH.[26] Consequently, these analysis results demonstrate that our photocatalysts are based on layered double hydroxide structures charge-neutralized between positive oxide layers and interlayer anions. Moreover, we found that the CNO^- ions exist in only the (Ni/Ti)LDH. All of the interlayer anions are considered to be generated *via* the decomposition of urea,[27] as summarized by the following two equations:

$$CO(NH_2)_2 \rightarrow NH_4CNO \quad (2)$$

$$NH_4CNO + 2H_2O \rightarrow 2NH^{4+} + CO_3^{2-} \quad (3)$$

Also, it could be interpreted from the previous studies[27,28] that the ammonium cyanate could decompose into ammonium chloride and cyanate ions since Cl^- ions have been used in the case of the (Ni/Ti)LDH (see eqn (4)), while there is no CNO^- band in the (Cu/Ti)LDH.

$$NH_4CNO + Cl^- \rightarrow NH_4Cl + CNO^- \quad (4)$$

Also, these reactions give a clue to the different crystallinity between (Ni/Ti)LDH and (Cu/Ti)LDH (see Fig. 2). The high electron density of cyanate ions would cause the high repulsion

force between the metal oxide layer and interlayer cyanate anions, thus resulting in the disordered crystalline structure for the (Ni/Ti)LDH that results in the broad XRD peaks.[28,29]

The elemental chemical analysis was performed for the materials using an inductively coupled plasma mass spectrometer (ICP-MS) for the materials to establish the composition and the atomic ratio of the metals. Table 1 summarizes the elemental information for these materials and shows that the M^{II}/Ti atomic ratio are 5.86 and 5.91 for (Ni/Ti)LDH and (Cu/Ti)LDH, respectively. These values are slightly lower than the molar ratio existing in the starting suspension. This phenomenon is attributed to a preferential precipitation of one cation as hydroxide.[30]

XPS analysis is performed to investigate the metal oxo-bridging LDH structures by comparing with the pure metal oxide. As shown in Fig. 4, there are a clear differences in each image. Every red line shows the M^{II+}–O–Ti^{4+} bonding and every black line shows the M^{II+}–O–M^{II+} bonding and M^{IV}–O–M^{IV} bonding[20] (Also see Fig. S2 for the detailed oxygen K-edged NEXAFS spectra†). The Ni 2p 3/2 peak has shifted to a low binding energy of 1.2 eV (Fig. 4(a)) and the Cu 2p 3/2 peak has shifted to a low binding energy of 1.4 eV (Fig. 4(b)) due to weaker bonding than that of pure oxide structures. The superposition of the Ni 2p 3/2 and the Cu 2p 3/2 at the low binding energy can be explained by the difference of the electronegativity between Ni/Cu and Ti; Ni/Cu has an electronegativity of 1.4 while Ti has 1.9. Therefore, the center of bonding of the Ni(or Cu)–O bonding has moved to the Ti side due to the different attraction forces between the metal and the oxygen. In addition, the Cu 2p 3/2 showed a larger superposition value than that of the Ni 2p 3/2 because of those compounds' different atomic numbers. The binding energy of the metal is defined by the positive potential caused by the specific arrangement of the ion core and the electrons. Because Cu has more protons than Ni, the binding energy of the Cu is larger than that of the Ni. Therefore, the decrease of the binding energy of Cu is higher than that of Ni even though the two materials have the same difference in the electronegativity compared with Ti. However, the two LDHs showed the same decreasing ratio of binding energy compared to the binding energy of their pure metal oxide structures.

The Ti 2p 3/2 peaks, illustrated in Fig. 4(c) and (d), are shifted to the lower binding energies of 3.8 eV in (Ni/Ti)LDH and 4.3 eV in (Cu/Ti)LDH. These shifted peaks are similar in energy to the binding energy of TiO and is attributed to the bonding nature of LDHs. Because the LDHs are made of metal octahedra, Ti^{4+} has a lack of oxygen, just like TiO^{2+}.[31,32] The charge neutrality is balanced by the interlayer anion, such as CO_3^{2-}, but the bonding of Ti–O looks like a TiO bonding where Ti exists in the center of the octahedron as Ti^{4+}. Consequently, these XPS data demonstrate that LDHs are composed of two metal centered octahedra and the octahedra are bonded to each other through the metal oxo-bridging.

The low temperature N_2 sorption analysis was conducted to confirm the suitability of the materials for use as a catalyst by studying the specific surface area, which can be the reaction site. Fig. 5 shows the N_2 sorption hysteresis loop of the materials at 77 K. The specific surface area, which is calculated by the BET method, is 187 $m^2\ g^{-1}$ for the (Ni/Ti)LDH and 85 $m^2\ g^{-1}$ for the (Cu/Ti)LDH. The value for the (Ni/Ti)LDH is about double that of the (Cu/Ti)LDH. This result implies that the (Ni/Ti)LDH would result in a better catalytic activity than that for the (Cu/Ti)LDH. In addition, the pore analysis for the two materials are performed; the results are shown in Fig. S1.† The pore size distribution of the two LDHs showed a similar value to the interlayer distance calculated from the (003) powder X-ray diffraction pattern.

The most important characteristic of the titanium embedded LDHs is the visible light absorption ability. Fig. 6 shows the UV-vis spectra for our newly synthesized LDHs. Both of two LDHs have absorption regions in the blue and the red regions. Therefore, the materials have a green color because they show a low efficiency of absorption in the green region. It has been know that the three types of metal oxide (NiO, CuO, TiO_2) showed improper absorption characters for water oxidation photocatalysts, except copper oxide.[33,34] However, the mixed hydrotalcites appeared to have totally different absorption spectra, so that they could be used to oxidize water. In the previous report, titanium was found not to influence the absorption ability of

Table 1 Summary of elemental analysis of the materials

Sample	Ti (wt%)	Ni (wt%)	Cu (wt%)	M^{II}/Ti ratio
(Ni/Ti) LDH	5.96	42.78	0	5.86
(Cu/Ti)LDH	5.51	0	43.21	5.91

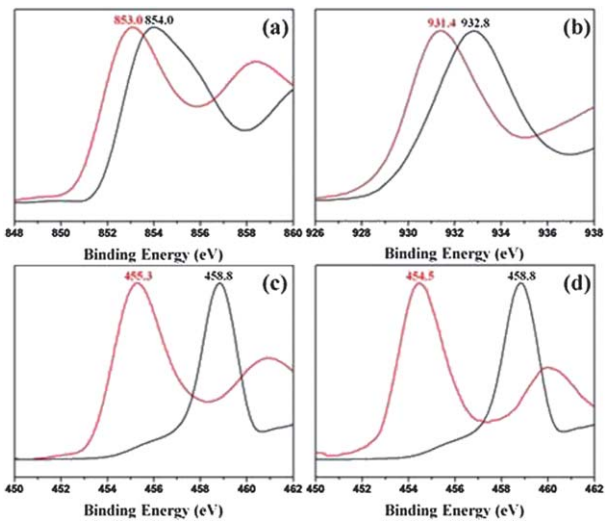

Fig. 4 XPS data for (a) Ni 2p 3/2, red: (Ni/Ti)LDH, black: NiO, (b) Cu 2p 3/2, red: (Cu/Ti)LDH, black: CuO, (c) Ti 2p 3/2, red: (Ni/Ti)LDH, black: TiO_2, (d) Ti 2p 3/2, red: (Cu/Ti)LDH, black: TiO_2.

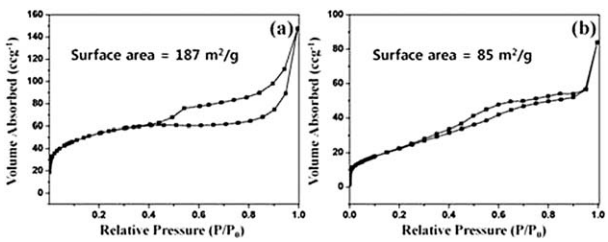

Fig. 5 N_2 sorption isotherms of (a) (Ni/Ti)LDH and (b) (Cu/Ti)LDH.

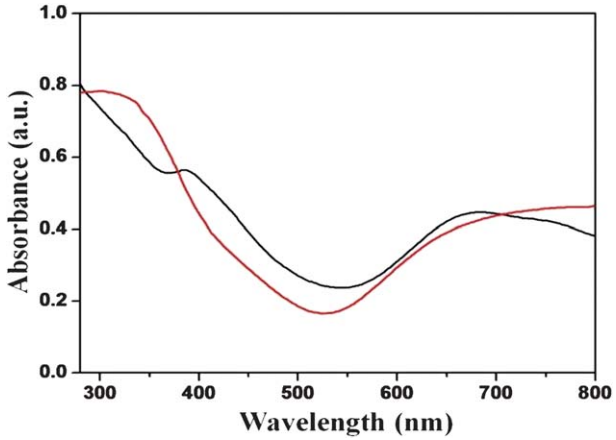

Fig. 6 UV-Vis spectra for (Ni/Ti)LDH in black and (Cu/Ti)LDH in red.

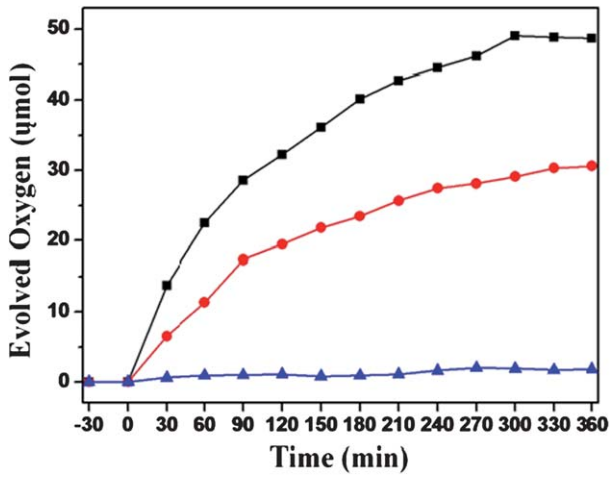

Fig. 7 Oxygen evolution in aqueous suspensions, black line shown with ■: (Ni/Ti) LDH, red line shown with ●: (Cu/Ti)LDH, blue line shown with ▲: TiO_2 nanoparticles.

a zinc-based LDH, but we found that this is not applicable in the cases of the (Ni/Ti)LDH and the (Cu/Ti)LDH.[22] In addition, it is determined that the (Ni/Ti)LDH is a better structure for the photocatalytic water oxidation as it absorbs a much larger amount of light in the visible light region than the (Cu/Ti)LDH.

As can be seen from Fig. 7, the oxygen molecules evolve by splitting of the water in the photocatalytic reaction with saturation values in long irradiation time. This saturation occurs due to the extinction of Ag^+ from $AgNO_3$, acting as a sacrificial agent, accepting electrons in order to prohibit the recombination between photocatalytically generated electrons and holes in the reaction. In addition, we also confirmed that there is no oxygen evolution when the reactor is not irradiated for 30 min as shown in Fig. 7.

(Ni/Ti)LDH showed a better water oxidation property than (Cu/Ti)LDH, as can be inferred from the UV-vis spectra and low temperature N_2 sorption data. The efficiency of (Ni/Ti)LDH for oxygen generation was found to be 1.6 times higher than that of (Cu/Ti)LDH. The aqueous suspension of (Ni/Ti)LDH produced 49 μmol in 5 h, while the suspension of (Cu/Ti)LDH produced 31

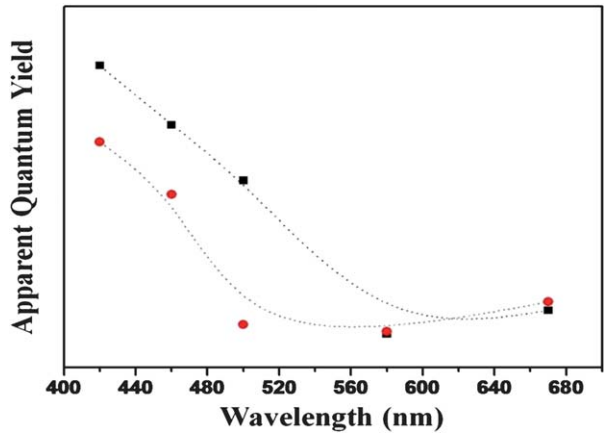

Fig. 8 Apparent quantum yields of LDH photocatalysts, black dotted line shown with ■: (Ni/Ti)LDH, red dotted line shown with ●: (Cu/Ti)LDH.

μmol. On the other hand, the normal TiO_2 generated a very small amount of oxygen within the error range because the TiO_2 does not have any absorption band in the visible light range.

We have further elucidated which part of the visible light is responsible for the water oxidation on two different LDH photocatalysts. In order to determine the apparent quantum yield for the specific part of visible light, we performed the photocatalytic reaction using 4 types of long pass filters (Hoya, Y44, Y48, O56, R64) and the air-cooled thermopile actinometer (Coherent, PM10 with FieldMaxII as power meter). Fig. 8 illustrates the results of the (Ni/Ti)LDH and the (Cu/Ti)LDH photocatalysts which show high quantum yields only in the blue light region. This indicates that blue light absorption is the main source of metal to metal charge transfer of two LDH materials.

In order to provide evidence for the sacrifice reaction of Ag^+ and to observe the structure of the two materials, we performed TEM analysis and EDX analysis for both LDHs; the results are provided in Fig. 9. The images taken before the photocatalytic reaction of the two materials show that the stacking of the layers is done in a plate shape. As can be seen in Fig. 9(c) and (d), which were taken after the photocatalytic reaction, significant amounts of nanoparticles are deposited on the surfaces of our new LDHs.

The compositions of these nanoparticles were found through the EDX analysis to be silver nanoparticles. These silver nanoparticles were created by accepting the electrons generated during the photocatalytic reaction. Therefore, the reason for the saturation effect during a long irradiation time is obviously established. Ag^+ is transferred into Ag nanoparticles and deposited on the surface of the photocatalyst from the start of the reaction, while the oxygen evolution is stopped when Ag^+ is completely exhausted after a long reaction time. It should be noted that the sacrificial Ag could be a problem to practical applications, but it is very useful to understand the evolution characteristics of O_2 from water at the same time.[35–38]

According to the data mentioned earlier, the amount of produced oxygen is found to be smaller than the ideal value that could be determined from the amount of $AgNO_3$. Because the concentration of $AgNO_3$ in the suspension is 1 M, the amount of generated oxygen would be 250 μmol (the suspension volume is

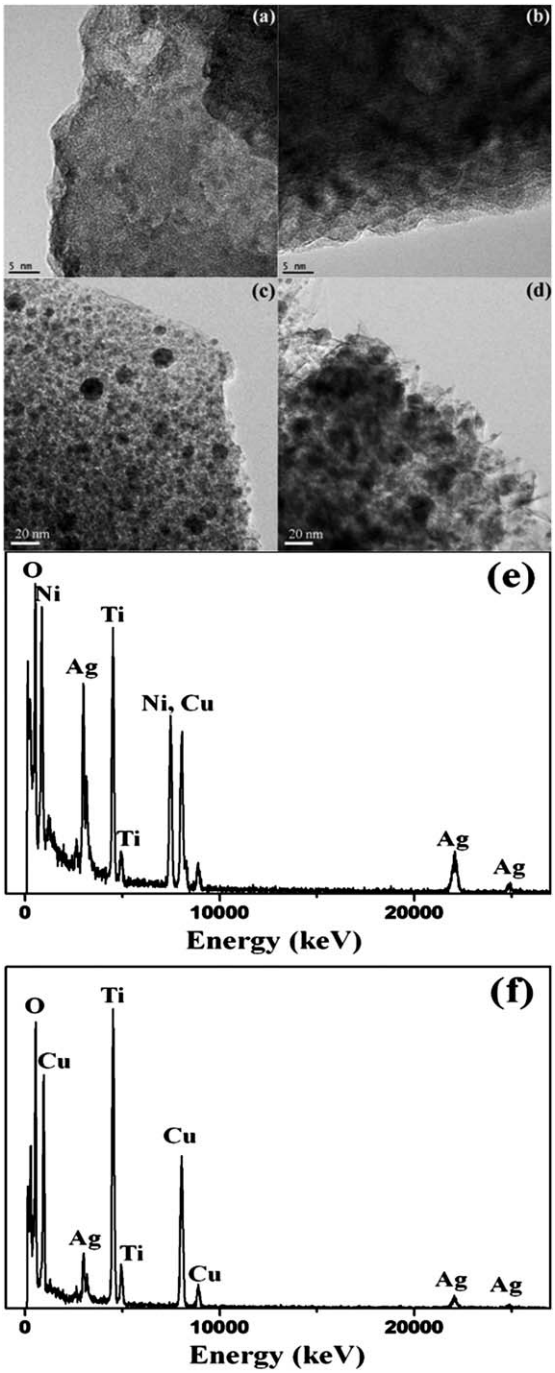

Fig. 9 TEM images of (a) (Ni/Ti) LDH before the reaction, (b) (Cu/Ti) LDH photocatalyst before the reaction, (c) (Ni/Ti) LDH photocatalyst after the reaction, (d) (Cu/Ti) LDH after the reaction, (e) EDX analysis of image (c), and (f) EDX analysis of image (d).

100 mL) if we assume that the oxidation of each water molecule requires four holes. However, we find that the (Ni/Ti) and (Cu/Ti) LDHs give about 50 μmol and 30 μmol, respectively. The reason for this phenomenon is very complicated so that it couldn't be concluded with one theory. Meanwhile, there have been several reports capable of providing a good clue to the reason why the produced oxygen from water is smaller than the ideal value. First of all, the oxygen generation rate on the surface of an oxide catalyst would be much slower than the reduction rate of the silver ion. Tang *et al.*[39] reported that the oxygen evolution from water takes nearly 1 s and Yamakata *et al.*[40] reported that Ag^+ can trap electrons in a few nanoseconds. Second, the photo-generated oxygen further reacts to form peroxotitanate at the surface of an oxide catalyst, such as TiO_2[41] and reacts with water to form H_2O_2,[42] in the solution. Moreover, the photo-generated oxygen is expected to remain adsorbed on the surface of an oxide catalyst and then act as a hole trap site by becoming a radical so that the oxide catalyst can absorb holes by itself.[43] For similar reasons, we consider that oxide structures of two (Ni/Ti) and (Cu/Ti) LDHs might have depressed the oxygen generation rates from water.

Comparing the photocatalytic efficiency to conventional photocatalysts, we selected the WO_3 nanoparticle which is a widely used photocatalyst for water oxidation, where the size of WO_3 nanopowders is less than 100 nm.[44] The water oxidation of WO_3 nanopowders was performed under the same conditions with our two LDHs. It was determined that the WO_3 generated 30 μmol of oxygen. This value is about 60% of that of the (Ni/Ti)LDH (see Fig. S3†). We also find that the high efficiency of this LDH is attributed to the good water sorption ability of a LDH on its large surface area.

Conclusions

We have reported new titanium embedded layered double hydroxides (LDHs) with large surface areas, such as (Ni/Ti)LDH and (Cu/Ti)LDH, that are very efficient for water oxidation under visible light. First of all, we found that the aqueous suspension of (Ni/Ti)LDH produced 49 μmol of oxygen using 200 mg of the photocatalyst and 1 mmol of $AgNO_3$ as a sacrificial agent, while the suspension of the (Cu/Ti)LDH produced 31 μmol. Furthermore, we investigated which part of the visible light is more effective for oxidizing water molecules by obtaining the apparent quantum efficiency. On the other hand, the normal TiO_2 generated a very small amount of oxygen within the error range. In addition, the structure of the LDHs and the bonding nature for a mixed oxide structure of LDHs are proved in this work. The two kinds of LDHs show two absorption bands in the red and blue regions under visible light, thus different from those of a pure metal oxide with absorption bands in only the UV region. We conclude that the absorption bands in the visible range and the large surface areas of LDHs have resulted in the high water oxidation photocatalytic activities under visible light.

Acknowledgements

This work was mainly supported by the Korea Center for Artificial Photosynthesis (KCAP) funded by the Ministry of Education, Science and Technology (NRF-2009-C1AAA001-2009-0093879). Y. Lee was supported by the Hydrogen Energy R&D Center from one of the 21st Century Frontier R&D Programs, and J. W. Lee was supported by the WCU program (R-31-2008-000-10055-0). Also, K. M. Choi was supported in part by grants from National Research Foundation (NRF-R0A-2007-000-20029-0) and J. H. Choi was supported in part by the Center for Inorganic Photovoltaic Materials (NRF-2010-0007692).

Notes and references

1 N. S. Lewis and D. G. Nocera, *Proc. Natl. Acad. Sci. U. S. A.*, 2006, **103**, 15729–15735.
2 D. G. Hetterscheid, J. I. Vlhgt, B. Bruin and J. N. H. Reek, *Angew. Chem., Int. Ed.*, 2009, **48**, 8178–8181.
3 A. Listorti, J. Durrant and J. Barber, *Nat. Mater.*, 2009, **8**, 929–930.
4 K. Maeda, T. Takata, M. Hara, N. Saito, Y. Inoue, H. Kobayashi and K. Domen, *J. Am. Chem. Soc.*, 2005, **127**, 8286–8287.
5 H. Tributsch, *Int. J. Hydrogen Energy*, 2008, **33**, 5911–5930.
6 K. Rangan, S. M. Arachchige, J. R. Brown and K. J. Brewer, *Energy Environ. Sci.*, 2009, **2**, 410–419.
7 J. Rosenthal, J. Bachman, J. L. Dempsey, A. J. Esswein, T. G. Gray, J. M. Hodgkiss, D. R. Manke, T. D. Luckett, B. J. Pistorio, A. S. Veige and D. G. Nocera, *Coord. Chem. Rev.*, 2005, **249**, 1316–1326.
8 H. Kato, K. Asakura and A. Kudo, *J. Am. Chem. Soc.*, 2003, **125**, 3082–3089.
9 H. G. Kim, D. W. Hwang, J. Kim, Y. G. Kim and J. S. Lee, *Chem. Commun.*, 1999, **13**, 1077–1078.
10 J. L. Dempsey, A. J. Esswein, D. R. Manke, J. Rosenthal, J. D. Soper and D. G. Nocera, *Inorg. Chem.*, 2005, **44**, 6879–6892.
11 A. J. Bard and M. A. Mary, *Acc. Chem. Res.*, 1995, **28**, 141–145.
12 G. Liu, L. Wang, H. G. Yang, H. M. Cheng and G. Q. Lu, *J. Mater. Chem.*, 2010, **20**, 831–843.
13 R. Asahi, T. Morikawa, T. Ohwaki, K. Aoki and Y. Tage, *Science*, 2001, **293**, 269–271.
14 S. Sakthivel and H. Kisch, *Angew. Chem., Int. Ed.*, 2003, **42**, 4908–4911.
15 S. S. U. M. Kahn, M. Al-shahry and W. B. Ingler, Jr, *Science*, 2002, **297**, 2243–2245.
16 J. Zhang, Y. Wu, M. Xing, S. A. K. Lighari and S. Sajjad, *Energy Environ. Sci.*, 2011, **3**, 715–726.
17 R. Nakamura and H. Frei, *J. Am. Chem. Soc.*, 2006, **128**, 10668.
18 W. Lin and H. Frei, *J. Phys. Chem. B*, 2005, **109**, 4929–4935.
19 W. Lin and H. Frei, *J. Am. Chem. Soc.*, 2005, **127**, 1610–1611.
20 R. Nakamura, A. Okamoto, H. Osawa, H. Irie and K. Hashimoto, *J. Am. Chem. Soc.*, 2007, **129**, 9596–9597.
21 C. G. Silva, Y. Bouizi, V. Fornes and H. Garcia, *J. Am. Chem. Soc.*, 2009, **131**, 13833–13839.
22 A. Kudo and Y. Miseki, *Chem. Soc. Rev.*, 2009, **38**, 253.
23 J. B. D. Calierie, M. Kermarec and O. Clause, *J. Am. Chem. Soc.*, 1995, **117**, 11471–11481.
24 K. T. Ehlsissen, A. Delahaye-Vidal, P. Genin, M. Figlaz and P. Willmann, *J. Mater. Chem.*, 1993, **3**, 883.
25 W. H. Zhang, X. D. Guo, J. He and Z. Y. Qian, *J. Eur. Ceram. Soc.*, 2008, **28**, 1623.
26 M. K. Titulaer, J. B. H. Jansen and J. W. Geus, *Clays Clay Miner.*, 1994, **42**, 249.
27 X. Shu, W. Zhang, J. He, F. Gao and Y. Zhu, *Solid State Sci.*, 2006, **8**, 634.
28 O. Saber, B. Hatano and H. Tagaya, *J. Inclusion Phenom. Macrocyclic Chem.*, 2005, **51**, 17.
29 X. Li, X. Zhang, Z. Li and Y. Qian, *Solid State Commun.*, 2006, **137**, 581–584.
30 O. Saber and H. Tagaya, *J. Incl. Phenom. Macropro.*, 2003, **45**, 109.
31 J. Dupin, D. Gonbeau, P. Vinatier and A. Levasseur, *Phys. Chem. Chem. Phys.*, 2000, **2**, 1319–1324.
32 S. Bartkowski and M. Neumann, *Phys. Rev. B: Condens. Matter*, 1997, **56**, 10656–10667.
33 M. Yin, C. K. Wu, Y. Lou, C. Burda, J. T. Koberstein, Y. Zhu and S. O'Brien, *J. Am. Chem. Soc.*, 2005, **127**, 9506–9511.
34 H. Irie, Y. Watanabe and K. Hashimoto, *J. Phys. Chem. B*, 2003, **107**, 5483–5486.
35 D. Chen and A. K. Ray, *Chem. Eng. Sci.*, 2001, **56**, 1561–1570.
36 L. Murruni, G. Leyva and M. I. Litter, *Catal. Today*, 2007, **129**, 127–135.
37 T. Aarthi and G. Madras, *Catal. Commun.*, 2008, **9**, 630–634.
38 K. Kabra, R. Chaudhary and R. L. Sawhney, *Environ. Prog.*, 2008, **27**, 487–495.
39 J. Tang, J. R. Durrant and D. R. Klug, *J. Am. Chem. Soc.*, 2008, **130**, 13885–13891.
40 A. Yamakata, T. Ishibashi and H. Onishi, *J. Phys. Chem. B*, 2001, **105**, 7258–7262.
41 J. Kiwi and M. Gratzel, *J. Phys. Chem.*, 1984, **88**, 1302–1307.
42 A. Patsoura, D. I. Kondarides and X. E. Verykios, *Appl. Catal., B*, 2006, **64**, 171–179.
43 A. L. Linsebigler, G. Lu and J. T. Yates, Jr., *Chem. Rev.*, 1995, **95**, 735–758.
44 R. Abe, T. Takata, H. Sugihara and K. Domen, *Chem. Commun.*, 2005, **19**, 3829–3831.

